Minute quantities of hexagonal nanoplates PtFe alloy with facile operating conditions enhanced electrocatalytic activity and durability for oxygen reduction reaction

Nannan Wang[1], Yanqiang Li[2], Zhanglin Guo[1], Huan Li[1], Shuzi Hayase[1], Tingli Ma*[1, 2]

[1]Graduate School of Life Science and Systems Engineering, Kyushu Institute of Technology, Wakamatsu, Kitakyushu, 808-0196, Japan

[2]School of Petroleum and Chemical Engineering, Dalian University of Technology, Panjin Campus, Panjin 124221, P. R. China

*Author to whom correspondence should be addressed. E-mail: tinglima@life.kyutech.ac.jp

Abstract

Pt-based alloys have been explored as the most promising cathode catalyst for fuel cells due to their excellent electrocatalytic activity in oxygen reduction reaction (ORR). However, the long-term performance of Pt-based alloys is compromised owing to the de-alloying behavior under the corrosive circumstance. More importantly, the complicated synthesized methods have hindered their further practical application. In this report, a facile and effective operating conditions-assisted method has been developed to synthesize the stable hexagonal nanoplates PtFe alloy with a high electrocatalytic activity. In the three prepared PtM (M: Fe, Co, Ni) alloy samples, the PtFe alloy exhibits a superior catalytic activity, which improves by about 100 and 178 mV for half-wave potential in alkaline and acidic medium with the same Pt-loading amount, respectively. In addition, the PtFe alloy catalyst exhibits an electrochemical stability, compared to the conventional carbon-supported Pt catalysts. In view of the advantages of the facile operating preparation and the excellent electrocatalytic

performance, we believe that the hexagonal nanoplates PtFe alloy holds great application as a promising electrocatalyst in polymer electrolyte membrane fuel cell (PEMFC).

Keywords: ORR catalysts; Pt-based alloys; Nanoplates; PEMFC.

1. Introduction

The polymer electrolyte membrane fuel cell (PEMFC) is recognized as the most effective and environmental-friendly technology for future clean energy [1]. However, the low natural abundance of Pt element and insufficient durability of Pt as the air electrode catalyst have greatly restricted their commercialization. Recently, the rational design of Pt alloys with different transition metals have been regarded as one of the most effective methods to obtain the highly active catalysts because of the high catalytic activity and Pt utilization rate. Among the various ORR catalysts that have been reported [2-10], the Pt alloys with Pt-late transition metals (Fe, Co, Ni, Cu, *etc*.) are the most widely studied because of their the richest reserve and the most abundant resource in the word. However, the major challenge for the wide commercialization of PEMFC lies in the high Pt-loading amount and the poor stability of Pt-based alloys in the ORR. Many Pt-based alloys are synthesized by transition metal deposition on Pt surface, leading to a high Pt-loading amount and no change on the d-band center of Pt. Conventionally, the poor stability of Pt-based alloys is caused by the de-alloying under the corrosive circumstances. Therefore, it is urgent to reduce or completely replace these low cost-effective and complicated methods in the catalyst preparation.

It is popular that Pt-based alloys maintain the most effective pathway (four-electron pathway) in the acidic or basic medium for ORR in the PEMFC. Most Pt-late transition metals have the advantages of shortening Pt-Pt bond distances and increasing the active surface area through their dissolution, changing the d-band center, and increasing the vacancy of Pt, which is beneficial for improving the electrochemical activity [11-18]. Among the different Pt-late transition metals, Fe, Co, and Ni are better than the others because they have adequate oxygen binding energy for the oxygen adsorption and desorption in the ORR process. [15-17, 19-22] Toda's group reported three sputtered bimetallic films PtM (M: Fe, Co, Ni) [23-24], and the PtFe sample shows the greatest enhancement in the activity of the catalyst. Samenkovic's group reported the electrocatalytic activity sequence of different metals in the order of $Pt<Pt_3Ti<Pt_3V<Pt_3Ni<Pt_3Fe\approx Pt_3Co$. [25] However, recently, Stamenkovic's group proved that Pt_3Co has the highest limited current density similar to Pt_3Ni [26], which is much higher than Pt_3Fe and different from the alloys activity order reported by their group. This different description confirmed that many variations are in the electrocatalytic activity sequence of the catalyst.

Many papers on catalysts based on Pt alloys with Fe, Co and Ni have been reported. Very recently, Huang et al. synthesized Pt_3Ni nanoparticles with the lowest Pt-loading amount in Pt alloys, which is comparable to commercial Pt/C with a 4.08 $\mu g_{Pt}/cm^2$ loading amount on the working electrode. [27] However, this method of synthesized may not be appropriate for large-scale production. More facile synthesized methods should be investigated and the lower Pt-loading amount also needs to be addressed.

Much more theoretical calculations and experiments have been carried out, the results confirmed that the morphology and size of the PtM nanoparticles have a great effect on their catalytic activity. [15, 27-29] Huang et al. found that the PtPb/Pt nanoplates show higher electrocatalytic activity than PtPb nanoparticles [28], due to that smaller nanoplates mean the higher surface area and much more the exposed active sites.

However, it is a challenge to obtain the nanoplates PtFe alloy with smaller size through a method that is suited for large-scale production. These features inspire us to explore: (1) Whether 2-D nanoplates can be synthesized by a facile method? (2) If it is possible, how to choose the precursor since the catalytic activity has a strong correlation with the precursor? (3) Can we significantly decrease the Pt-loading amount while retaining the high electrochemical activity?

We now report a facile synthesis route to prepare the hexagonal nanoplates PtFe alloy with a real low Pt content. The PtFe alloy shows a well-defined homogeneous hexagonal nanoplates structure, and ultra-small particle size (ca. 2.6 nm). When used as the ORR catalyst, the PtFe alloy shows a superior catalytic activity in comparison to the commercial Pt/C. Our study showed that the PtFe alloy catalyst has a great application potential as a substitute for the commercial Pt/C.

2. Experimental

2.1. Synthesis of the PtM (M: Fe, Co, Ni) catalysts

The PtM (M: Fe, Co, Ni) catalysts were synthesized by a simple one-step solvent reduction method. In a typical procedure, 0.015 mmol of chloride

metal was dissolved in 10 mL of the formic acid (CH_2O_2, 98-100%, WAKO®) by slowly stirring for 1 hour then forming the core solution. Then 1.5 ml of the 0.2 mmol/L $H_2PtCl_6 \cdot 6H_2O$ solution (corresponding to 0.0585 mg_{Pt}) was dissolved in 13.5 ml of ultrapure water. This solution was added to the core solution to form a clear liquid. Finally, 1.22 g of formic acid as the reductant and 18 mg of carbon black as the support were fed into the PtM (M: Fe, Co, Ni) solution. After vigorously stirring for 24 hours, the resulting catalyst powder was filtered out, washed several times with ultrapure water and dried at 60 ^oC for further characterization.

2.2. Physical characterizations

The powder X-ray diffraction (XRD) was recorded by a Rigaku diffractometer using Cu *Kα* radiation (λ= 1.54056 Å) with a scanning speed of 5° min^{-1} from 10° to 70°. The morphology and microstructure of the samples were analyzed by transmission electron microscopy and TEM-EDS (Tecnai G2 F20 S-TWIN). X-ray photoelectron spectroscopy (XPS, Thermo Escalab 250Xi) was conducted to analyze the surface status of the chemical elements.

2.3. Electrochemical measurements

The catalytic tests were performed using a standard three-electrode system with a rotating disk electrode (RDE) setup from Pine Instrument Company connect to a CHI 760E electrochemistry workstation. A glassy carbon disk (5-mm diameter) was used as the working electrode, Ag/AgCl as the reference electrode and a platinum wire as the counter electrode. For the preparation of the working electrode, 6 mg of the sample and a Nafion

solution (5 wt. %, 0.1 ml) were mixed with ultrapure water (0.15 ml) and isopropanol (IPA, 0.25 ml) ultrasonically for more than 0.5 hours. 8 µl of a catalyst ink was then transferred to the GC electrode to reach a loading amount of 489 $\mu g/cm^2$ (corresponding to a 3.48 $\mu g_{Pt}/cm^2$ loading on the working electrode, thus no loss in the experiment process). As a comparison, 4 mg of 20% Pt/C was mixed with a Nafion solution (5 wt. %, 0.1 ml), ultrapure water (0.8 ml) and IPA (1.1 ml) ultrasonically for more than 0.5 h, keeping 102.04 $\mu g/cm^2$ (corresponding to 20.41 $\mu g_{Pt}/cm^2$) on the GC electrode.

The cyclic voltammetry (CV) was recorded in acidic medium (the potential range 1.21~ 0.02 V *vs*. RHE) and in basic medium (the potential range 1.23 ~ 0.03 V *vs*. RHE) with the scan rate of 10 mV/s in nitrogen and/or oxygen saturated 0.1 M $HClO_4$ and/or 0.1 M KOH solutions at room temperature. The stability of the sample PtFe alloy measurement is the same as the CV test, except for the scan rate of 50 mV/s for 700 cycles and only in the oxygen-saturated solution. The working electrode was cycled at least five times before the data recorded in all CV tests.

The linear sweep voltammetry (LSV) was recorded in acidic medium (the potential range 1.40 ~ 0.18 V *vs*. RHE) and in basic medium (the potential range 1.43 ~ 0.26 V *vs*. RHE) with the scan rate of 10 mV/s in oxygen-saturated 0.1 M $HClO_4$ or 0.1 M KOH solutions at room temperature with the different rotating speeds from 625 to 2500 rpm by using a Pine Instruments device. It should be noted that all the potentials have been iR-corrected.

The electrochemical impedance spectroscopy (EIS) measurement was recorded for the samples in a frequency range of 100 kHz to 1Hz in the

basic and acidic medium at open circuit voltage. For the Tafel plot, the kinetic current was calculated from the mass transport correction of the LSV curve by the following equation:

$$J_K = (J \times J_L) / (J_L - J)$$

In the equation, J is the measured current density on the GC disk, and J_K and J_L are the kinetic and diffusion limited current densities, respectively.

3. Results and discussion

Powder X-ray diffraction was carried out to evaluate the formation of the PtM (M: Fe, Co, Ni). As shown in Figure 1, broad peaks at ca. 25° and 43° can be detected, which correspond to the (002) and (100) plane of the graphite-like crystalline structure of the carbon support (ICDD No. 00-001-0640). Three diffraction peaks assigned to the Pt (ICDD No. 01-088-2343) (111), (200) and (220) planes were observed, which represents the typical feature of the face-centered cubic (fcc) polycrystalline Pt. No peaks of the pure M metals or MCl appeared in the XRD pattern, probably due to the M atoms percolating through the Pt crystalline, or the M atoms are too few to be detected by the X-rays. The weak and wide diffraction peaks of Pt are in the PtFe alloy sample due to the poor crystallinity and ultra-small nanoparticles. The calculated the relative intensity of the (111) and (200) face is ca. 1.19, which is larger than the standard 1.07 from the standard PDF card (ICDD No. 01-088-2343), suggesting the preferential growth direction. According to the earlier report, the shapes of Pt nanocrystals are

usually defined by cubic or other polyhedral that is enclosed by (111) and (100) facets [30], corresponding to the XRD pattern. This was also demonstrated by the ca. 0.47°, 0.40° and 0.32° positive shifts for PtFe, PtCo, PtNi alloys compared to the XRD cards of the pure Pt (39.27°), as shown in Figure 1, suggesting that the crystal structure changed compared to the pure Pt. This proved the M atoms were incorporated into the Pt structure during the synthesis, forming an M-Pt biometrical into the nanoparticles, as previously reported for Pt-skin nanoparticles [31].

Figures 2(a-d) are the bright field images of the typical transmission electron microscopic (TEM) and their particle size histograms of PtFe alloy. It can be clearly seen that the PtFe nanoplates were well dispersed on the black carbon (Figures 2a) and the average particle size is about 2.6 ± 0.5 nm (Figure 2d). The small particle size is believed to be very beneficial for enhancing the catalytic activity of the Pt. A high-resolution TEM micrograph (Figures 2b) shows the crystalline lattice spaces in two directions of 0.1940 and 0.2233 nm, respectively, which is lower than the lattice of the Pt (ICDD No. 01-088-2343) (200) (0.1985 nm) and (111) (0.2292 nm) facets. Figure 2c is the selected area electron diffraction (SAED), illustrating that the PtFe alloy is polycrystalline, and corresponds to the (110), (100) and (111) planes of the Pt crystal.

Figure 3 depicts the transmission electron microscopic-energy dispersive spectrometer (TEM-EDS) images of the PtFe product. The Pt: Fe atomic ratio was estimated to be 90.24: 9.76 from the TEM-EDS analysis. The observed Fe content in the PtFe alloy is much lower than the Fe content in the raw material of the Pt and Fe reagents, suggesting that the precursor

Fe^{3+} was only partially reduced to Fe atoms in the reaction. Combined with the XRD and TEM results, we believe that Fe atoms were incorporated into the Pt crystal.

XPS was used to analyze the valence states of the different elements in the PtFe catalyst. As shown in Figure 4a, three obvious peaks centered at 75, 284.3, and 533 eV can be observed, corresponding to the C 1s, Pt 4f and O 2p (Figure S1) signals, respectively. Two signals of Pt 4f: $4f_{7/2}$ and $4f_{5/2}$ were detected in the high-resolution Pt 4f peak, as shown in the inserted images of Figure 4a, indicating that the PtFe alloy is made of the Pt-rich structure on the surface. The peaks can be further divided into four peaks at the binding energies of 71.4, 74.8 and 72, 75.7 eV, which identified the different oxidation states of Pt. The former two belongs to Pt^0 and the latter two are assigned to Pt^{2+} species, such as PtO.

However, there are no Fe 2p orbits peaks, which can be detected by XPS, shown in Figure 4b. That is due to lack of Fe atoms on the surface of PtFe nanoplates. Another reason is the limitation of the equipment, the XPS can only detect several atomic layers from the surface, which means that there is almost none Fe atoms in the surface of the PtFe nanoplates according to previous reports [23, 24].

The ORR catalytic activity of the PtFe alloy catalyst (Figure 5a) in an alkaline medium was first explored by cyclic voltammetry (CV) in 0.1 M KOH at the scan rate of 10 mV/s. From the Figure 5a, there are no obvious reduction peaks, but an anodic peak at ca. 0.3 V in the CV curve in the N_2-saturated electrolyte, which was determined as hydrogen evolution peak. However, a pronounced cathodic peak at 0.91 V versus RHE in an O_2-

saturated solution can be observed, suggesting the high electrocatalytic activity of PtFe alloy. The PtNi and PtCo alloys also show similar behaviors (Figure S3). Of the three samples, the PtFe alloy catalyst shows a more positive cathodic peak in the O_2-saturated solution compared to the PtCo and PtNi alloys, implying its superior electrocatalytic activity. Linear sweep voltammetry (LSV) was conducted to further explore the electrocatalytic performance of the materials. The prominent current-voltage polarizations in Figure 5b once again reveal its high catalytic activity. The onset potentials, half-wave potentials and limiting current density obtained from the RDE measurements are listed in Table 1. Among all the samples, the PtFe alloy showed the highest onset potential of ca. 0.95 V *vs* RHE, indicating its higher catalytic performance than the other two samples, and this is consistent with the results from the CV measurements. In contrast, the onset potential of the PtNi and PtCo alloys catalysts shifted negative, implying a lower electrochemical activity. In general, the types of transition metals have great influences on the electrochemical activity. As previously reported [32], the onset potential of different transition metals decreases with the increasing dissolution potential of the metal which is the thermodynamic potential for the metal dissolution at pH=0. It should be noted that the limited current density of the PtFe alloy is about 11.43 times of commercial Pt/C catalyst at 0.95 V for the same Pt loading amount (Figure S5a).

A Koutecky–Levich (K–L) analysis of the PtFe alloy was performed to further investigate the catalyst kinetics by rotating disk electrode measurement at various rotating speeds (Figure 5c). The electron transfer

number of the PtFe alloy calculated from the K-L plot varied from 3.73 to 3.85 in the potential range of 0.3-0.7 V, suggesting a dominated the four-electron pathway of the ORR process. The number of electrons transfer for PtNi (Figure S2) and PtCo (Figure S2) was 2.93-3.14 and 3.55-4.05, respectively, in the range of 0.3-0.7 V, which is implying that all the samples obey the four-electron pathway in the ORR process.

Besides the high catalytic activity, the stability is another core parameter for the ORR catalyst (Figure 5d). The electrochemically-active surface area (ECSA) values are normalized by the initial ECSA determined for the titled samples as a function of the number of potential cycles. The cathode peak is another parameter to estimate the stability of the samples. It shifted due to the transition metals would dissolve and inactivate in the process. From the inset of Figure 5d, it clearly shows the cathode peak shifted a lot before 400 cycles. However, after 400 cycles, both the ECSA and the cathodic peak only slightly change little, which is illustrating its high stability.

Furthermore, the Tafel slope was explored to confirm the kinetics of the PtFe alloy in Figure 6a. It is known that a low Tafel slope is essential to obtain a high current at a low overpotential. Figure 6a shows that the Tafel slope of the PtFe alloy is 67 mV per decade. This confirmed that the first transfer electron is the rate-determining step in the ORR process, according to a previous report[33], the Tafel slope being close to $-2.303RT/aF \approx 60$ mV per decade (R is the molar gas constant, T is absolute temperature, a is transfer coefficient and F means Faraday constant) at room temperature. The Tafel slope is about 55 and 61 mV per decade for the PtCo and PtNi samples (Figure 6a), respectively.

It is known that the lower electron transfer resistance can facilitate the electron transfer ability. The electronic impedance spectroscopy (EIS) spectra were obtained to calculate the electron transfer resistance (Figure 6b). From Figure 6b, it is obvious that the electron transfer impedance of R1 for the ORR is about 22.48, 27.72 and 29.50 ohms for PtM (M: Fe, Co, Ni) samples, respectively. It should be noted that R_S is about 15 ohm for the three samples, thus we believe they should belong to solution resistance. The lower resistance value indicates the superior electron transfer ability in the ORR, which can enhance the ORR process. In order to analyze the correlation between the resistance and activity of the materials, we try to found a unique shape which is similar to the famous volcano shape [34]. Combined with the CV and LSV data, the onset potential and half-wave potential of these three samples increased with the low resistance value (correlation of the onset potential, half-wave potential, and limited current with the resistance value in Figure S 5a, S 6a, and S 7a). It should be noted that the electrochemical activity exhibits a similar inverse relationship with the resistance law (Figure S 5a). This suggests that the higher onset potential for the ORR with respect to the other transition metal alloyed with Pt is directly related to their lower resistance.

The PtM (M: Fe, Co, Ni) alloys also displayed a high catalytic activity for the ORR in 0.1 M $HClO_4$ medium. As shown in Figure 7a, the CV curves had a rectangular shape without any peak in the N_2-saturated electrolyte. Nevertheless, a clear oxygen reduction peak can be observed in the presence of oxygen at 0.72 V.

The catalytic performance of all the samples in acidic medium is summarized in Table 2. It is clear that the PtFe alloy catalyst illustrates the best electrochemical activity in view of the limited current density of the three samples of ca. 6.06 mA/cm^2 at 3.48$\mu g_{Pt}/cm^2$, while that is 5.15 mA/cm^2 at 20.41 $\mu g_{Pt}/cm^2$ for the Pt/C catalyst (Figure 7b). Except for the limited current density, the onset potential of the PtFe alloy is also more positive than the other two samples and even comparable to the commercial Pt/C catalyst. Similarly, we also found that the limited current density of the PtFe alloy is about 18.53 times of the commercial Pt/C catalyst at 0.7 V for the same Pt loading amount in acidic medium (Figure S4b).

The ORR mechanism of the PtFe alloy catalyst in 0.1 M $HClO_4$ was also investigated by an RDE measurement (Figure 7c). The K-L equation was introduced to analyze the transfer number of the reaction. The transfer number was estimated to be 3.79-4.26 per O_2 molecule at 0.2-0.6 V, suggesting that the oxygen reduction reaction mainly follows the four-electron pathway. Moreover, the number of electrons transfer for the PtNi (Figure S3d) and PtCo (Figure S3c) alloy catalysts were 4.46-4.99 and 3.84-4.05 in the range of 0.2-0.6 V, which is implying all the samples obey the four electrons pathway in the ORR process.

The stability of the PtFe alloy in acidic medium was also studied by the CV curves shown in Figure 7d and inset of Figure 7d. There is no obvious decrease on the ECSA and shifted the cathode peak after 400 cycles in the CV curves, indicating that the PtFe has a superior stability in acidic medium.

The Tafel slope of the PtFe alloy was essential to confirm the kinetics of the ORR in Figure 8a. Figure 8a shows the Tafel slope of the PtFe alloy which is 62 mV per decade, suggesting that the first transfer electron is the rate-determining step in the ORR process at room temperature. We also obtained the Tafel slope of the PtCo and PtNi alloys (Figure 6e) are about 71 and 93 mV per decade, respectively.

In order to explain the mechanism of the higher catalytic activity in the 0.1 M $HClO_4$ medium, we also investigated the electron transfer resistance of three samples (Figure 8b). From Figure 8b, we found that the electron transfer impedance R_1 for the ORR is about 46.37, 192.2 and 317.2 ohms for the PtM (M: Fe, Co, Ni) samples, respectively. It should be noted that R_S is about 9 ohm for the three samples, and we believe they should belong to solution resistance. The similar inverse relationship between the electrochemical activity and resistance also can be found in the acid solution. Combined with the CV and LSV data, the onset potential, half-wave potential and the limited current density of these three samples exhibit a linear relationship with the electron transfer impedance R_2 (correlation of the onset potential, half-wave potential and the limited current density with resistance value of Figure S5b, S6b and S7b)[33]. The negative relationship between the ORR activity and the R_2 suggests that the transition metal Fe alloyed with Pt contributed to improving the ORR catalytic activity.

Briefly, the PtFe alloy catalyst shows the best electrochemical activity among the PtM (M: Fe, Co, Ni) samples both in acidic and basic medium, which is a promising candidate to substitute for the commercial Pt/C

catalyst. This is due to that the Fe atoms are confined in the Pt crystal lattice without any lattice strain with increasing the transport of electrolyte and preventing dissolution of the active site. There is no doubt that the catalyst activity has a strong correlation with the precursor inorganic salt. Kapoor's group found that iron chloride reacts with formic acid to give the stable polymeric compound $FeCl(OOCH)_2 \cdot H_2O$ at room temperature [35]. With the help of the strongly reductive and acidic, Fe^{3+} would be reduced into Fe atoms. Furthermore, many groups demonstrated that formic acid can improve the electrochemical activity during preparation because it maintains a low overpotential and decreases the accumulation of intermediates on the catalyst surface [36, 37].

And there is another reason for its high electrochemical activity. The Sanjeev Mukherjee group [38] also verified that the electrocatalytic activity exhibited a volcano shape (PtFe>PtCo>PtNi) which has a relation to the Pt d-band vacancy per atom and Pt-Pt bond distance. As reported before, the dissociation of O_2 for the four-electron reduction can be clarified by two models, i.e., the Griffiths- and Bridged-type adsorptions. This paper introduces the Griffith's model for brevity, which involves a lateral interaction of the 2p orbitals of the O_2 with an empty 5dz2 orbital of a surface Pt atom with back bonding from the partially filled 5dxz or 5dyz orbital of Pt to the 2p orbitals of the O_2. [23, 39] Different late-transition metals doped into the crystalline of Pt can increase the vacancies of the Pt surface due to the fact that the late-transitions have more 5d vacancies than Pt, which has been confirmed by the previous reports. [11. 25] In other words, the 2p electron transfer from O_2 to the Pt surface increases with more 5d

vacancies, leading to an increased O_2 adsorption and weakening of the O-O bond, which increases the O_2 reaction rate. In short, the large d vacancy contributed to enhancing the O-O bond break. Meanwhile, the small particle size of 2.6 ± 0.5 nm can also greatly increase the activity of the samples.

Conclusions

In conclusion, PtM (M: Fe, Co, Ni) alloy samples as the effective ORR catalysts were synthesized using a simple method under the mild condition. The well-defined morphology, homogeneous and ultra-small particle size (ca. 2.6 nm) greatly contributed to their high catalytic activity. Advanced electrochemical analyses indicated that the PtFe alloy catalyst exhibits the best activity and superior electrochemical stability both in acidic and basic medium, probably due to the reason that the Fe atoms have more 5d orbitals than the other two metals. The facile synthesis procedure and the high catalytic activity make the PtFe alloy catalyst very promising to replace the commercial Pt/C catalyst as an ORR catalyst for fuel cells.

Acknowledgments

This work was supported by the Grant-in-Aid for Scientific Research (KAKENHI) program, Japan (C, Grant Number 15K05597) and Takahashi Industrial and Economic Research Foundation (Takahashi Grant Number 06-003-154).

References

[1] M. Shao, Q. W. Chang, J. Dodelet, R. Chenitz, Chem. Rev. 116 (2016) 3594-3657.

[2] R. J. Cui, L. Mei, G. J. Han, J. Y. Chen, G. H. Zhang, Y. Quan, N. Gu, L. Zhang, Y. Fang, B. Qian, X. F. Jiang, Z. D. Han, Scientific Reports 7 (2017) 41826.

[3] I. E. L. Stephens, A. S. Bondarenko, U. Gronbjerg, J. Rossmeisl, I. Chorkendorff, Energy Environ. Sci. 5 (2012) 6744-6762.

[4] P. Strasser, S. Koh, T. Anniyev, J. Greeley, K. More, C. F. Yu, Z. C. Liu, S. Kaya, D. Nordlund, H. Ogasawara, M. F. Toney, A. Nilsson, Nat. Chem. 2 (2010) 454-460.

[5] H. Y. Park, T. Y. Jeon, J. H. Jang, S. J. Yoo, K. H. Choi, N. Jung, Y. H. Chung, M. Ahn, Y. H. Cho, K. S. Lee, J. Electrochem. Acta 228 (2017) 389-397.

[6] Y. J. Wang, D. P. Wilkinson, A. Guest, V. Neburchilov, R. Baker, F. Nan, G. A. Botton, J. Zhang, J. Power Sources 221 (2013) 232-241.

[7] R. Balgis, W. Widiyastuti, T. Ogi, K. Okuyama, ACS Appl. Mater. Interfaces 9 (2017) 23792-23799.

[8] M. Escudero-Escribano, P. Malacrida, M. H. Hansen, U. G. Vej-Hansen, A. Velázquez-Palenzuela, V. Tripkovic, J. Schiøtz, J. Rossmeisl, I. E. L. Stephens, I. Chorkendorff, Science 352 (2016) 73-76.

[9] T. Fu, J. Fang, C. Wang, J. Zhao, J. Mater. Chem. A 4 (2016) 8803-8811.

[10] Antolini, E. Appl. Catal. B Environmental 74 (2007) 324-336.

[11] E. J. Coleman, M. H. Chowdhury, A. C. Co, ACS Catal. 5 (2015) 1245-1253.

[12] I. E. L. Stephens, A. S. Bondarenko, U. Gronbjerg, J. Rossmeisl, I. Chorkendorff, Energy Environ. Sci. 5 (2012) 6744-6762.

[13] N. E. Sahin, T. W. Napporn, L. Dubau, F. Kadirgan, J. M. Léger, B. K. Kokoh, Appl. Catal. B Environmental 203 (2017) 72-84.

[14] M. Ammam, E. B. Easton, J. Power Sources 236 (2013) 311-320.

[15] X. X. Du, Y. He, X. X. Wang, J. N. Wang, Energy Environ. Sci. 9 (2016) 2623-2632.

[16] S. P. Lin, K. W. Wang, C. W. Liu, H. S. Chen, J. H. Wang, J. Phys. Chem. C 119 (2015) 15224-15231.

[17] X. Huang, Z. Zhao, L. Cao, Y. Chen, E. Zhu, Z. Lin, M. Li, A. Yan, A. Zettl, Y. M. Wang, X. Duan, T.im Mueller, Y. Huang, ACS Appl. Mater. Interfaces 9 (2017) 9584-9591.

[18] H. D. El, M. Bron, J. Power Sources 275 (2015) 893-900.

[19] M. T. Nguyen, R. H. Wakabayashi, M. Yang, H. D. Abruña, F. J. Disalvo, J. Power Sources 280 (2015) 459-466.

[20] E. Pizzutilo, J. Knossalla, S. Geiger, J. P. Grote, G. Polymeros, C. Baldizzone, S. Mezzavilla, M. Ledendecker, A. Mingers, S. Cherevko, F. Schüth, K. J. J. Mayrhofer, Adv. Energy Mater. 2017, 1700835.

[21] G. Shi, H. Yano, D. A. Tryk, A. Iiyama, H. Uchida, ACS Catalysis 7 (2016) 267-274.

[22] S. Bhattacharjee, S. J. Yoo, U. V. Waghmare, S. C. Lee, Chemical Physics Letters 648 (2016) 166-169.

[23] T. Toda, H. Igarashi, H. Uchida, M. Watanabe, J. Electrochem. Soc. 146 (1999) 3750-3756.

[24] X. Ding, S. Yin, K. An, L. Luo, N. Shi, Y. H. Qiang, S. Pasupathi, B. G. Pollet, P. K. Shen, J. Mater. Chem. A 3 (2015) 4462-4469.

[25] V. R. Stamenkovic, B. S. Mun, M. Arenz, K. J. Mayrhofer, C. A. Lucas, G. Wang, P. N. Ross, N. M. Markovic, Nat. Mater. 6 (2007) 241.

[26] C. Wang, N. M. Markovic, V. R. Stamenkovic, ACS Catalysis 2 (2012) 891-898.

[27] X. Q. Huang, Z. P. Zhao, L. Cao, Y. Chen, E. B. Zhu, Z. Y. Lin, M. F. Li, A. M. Yan, A. Zettl, Y. M. Wang, X. F. Duan, T. Mueller, Y. Huang, Science 348 (2015) 1230-1234.

[28] L. Z. Bu, N. Zhang, S. J. Guo, X. Zhang, J. Li, J. L. Yao, T. Wu, G. Lu, J. Y. Ma, D. Su, X. Q. Huang, Science 354 (2016) 1410-1414.

[29] L. K. Wang, Z. H. Tang, W. Yan, Q. N. Wang, H. Y. Yang, S. W. Chen, J. Power Sources 343 (2017) 458-466.

[30] N. Tian, Z. Y. Zhou, S. G. Sun, Y. Ding, Z. L. Wang, Science 316 (2007) 732-735

[31] D. Wang, H. L. Xin, R. Hovden, H. Wang, Y. Yu, D. A. Muller, F. J. Disalvo, H. D. Abruna, Nat. Mater. 12 (2013) 81-87.

[32] B. H. Han, C. E. Carlton, J. Suntivich, Z. C. Xu, S. H. Yang, J. Phys. Chem. C 119 (2015) 3971-3978.

[33] Y.Li, W. Zhou, H. Wang, L. Xie Y. Liang, F. Wei, J. C. Idrobo, S. J. Pennycook, H. Dai, Nat. Tech. 7 (2012) 394-400.

[34] L. J. Li, P. C. Dai, X. Gu, Y. Wang, L. T. Yan, X. B. Zhao, J. Mater. Chem. A 5 (2017) 789-795.

[35] R. C. Paul, O. B. Baidya, A. J. Kaur, R. D. Sharma, R. Kapoor, Aust. J. Chem. 30 (1977) 1439-1443.

[36] L. S. R. Silva, E. L. Franz, M. Perez-Cadenas, S. F. Santos, L. P. da Costa, K. I.B. Eguiluz, G. R. S. Banda, Appl. Catal. B Environmental 198 (2016) 38-48.

[37] V. Juan, S. Jose, H. Enrique, M. Carlos, Appl. Catal. B Environmental 201 (2017) 48-57.

[38] S. Mukerjee, S. Srinivasan, M. P. Soriaga, J. McBreen, J. Electrochem. Soc. 142 (1995) 1409-1422.

[39] E. Yeager, M. Razaq, D. Gervasio, A. Razaq, D. Tryk, in: D. Scheerson, D. Tryk, M. Daroux, X. Xing (Eds.), Structural Effects in Electrocatalysis and Oxygen Electrochemistry, Proc. vol. 92-11, The Electrochemical Society Inc., Pennington, NJ, 1992, p. 440

Table 1. The ORR performance of different catalysts in alkaline medium

Samples	**PtFe**	**PtCo**	**PtNi**	**Pt/C (20.4 $\mu g_{Pt}/cm^2$)**	**Pt/C(3.48 $\mu g_{Pt}/cm^2$)**
Onset potential (V)	0.95	0.94	0.93	0.97	0.90
Half wave potential (V)	0.88	0.83	0.82	0.86	0.78
Diffusion limiting current (mA/cm^2)	5.83	5.66	4.55	5.67	4.40
Electron transfer number at 0.5V	3.73	3.59	2.93	4.00	4.00

Table 2. The ORR performance of different catalysts in acidic medium

Samples	**PtFe**	**PtCo**	**PtNi**	**Pt/C (20.4 $\mu g_{Pt}/cm^2$)**	**Pt/C(3.48 $\mu g_{Pt}/cm^2$)**
Onset potential (V)	0.75	0.74	0.73	0.75	0.69
Half wave potential (V)	0.70	0.67	0.63	0.67	0.52
Diffusion limiting current (mA/cm^2)	6.06	4.82	4.10	5.15	4.30
Electron transfer number at 0.5V	3.84	3.88	4.61	4.00	4.00

Scheme 1. Synthesis of PtFe followed through the soft chemistry method.

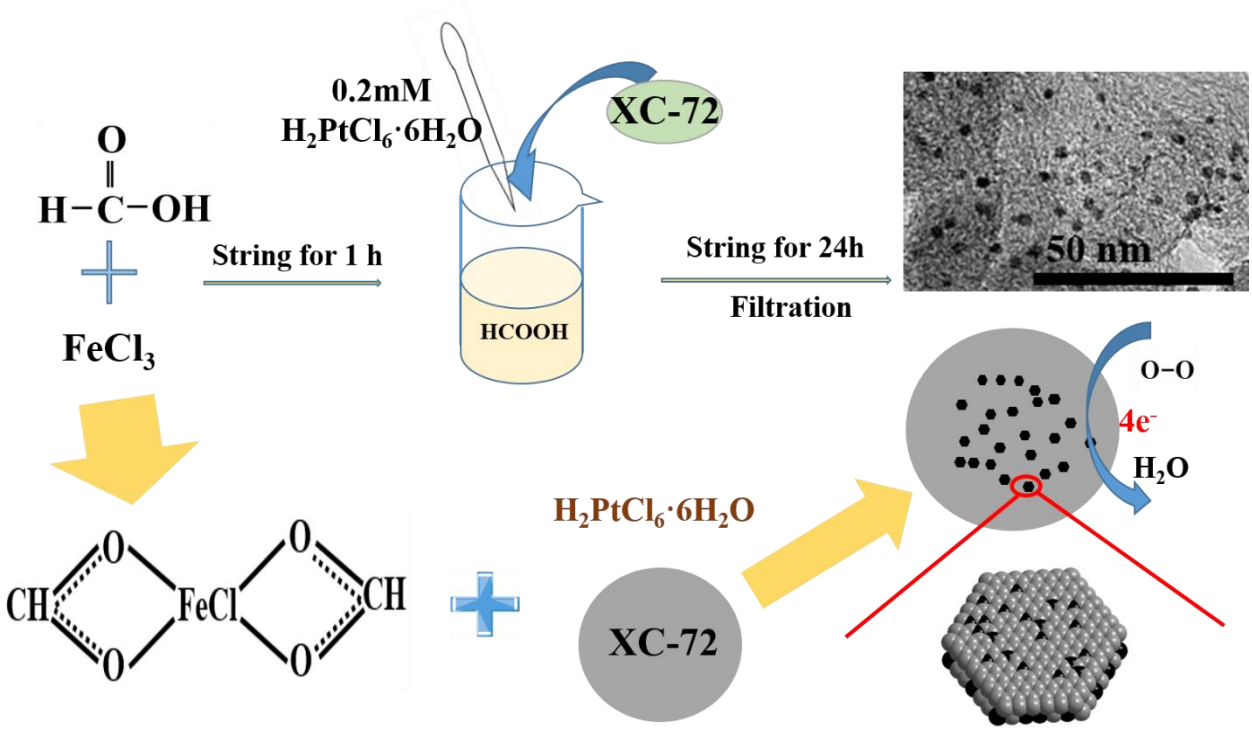

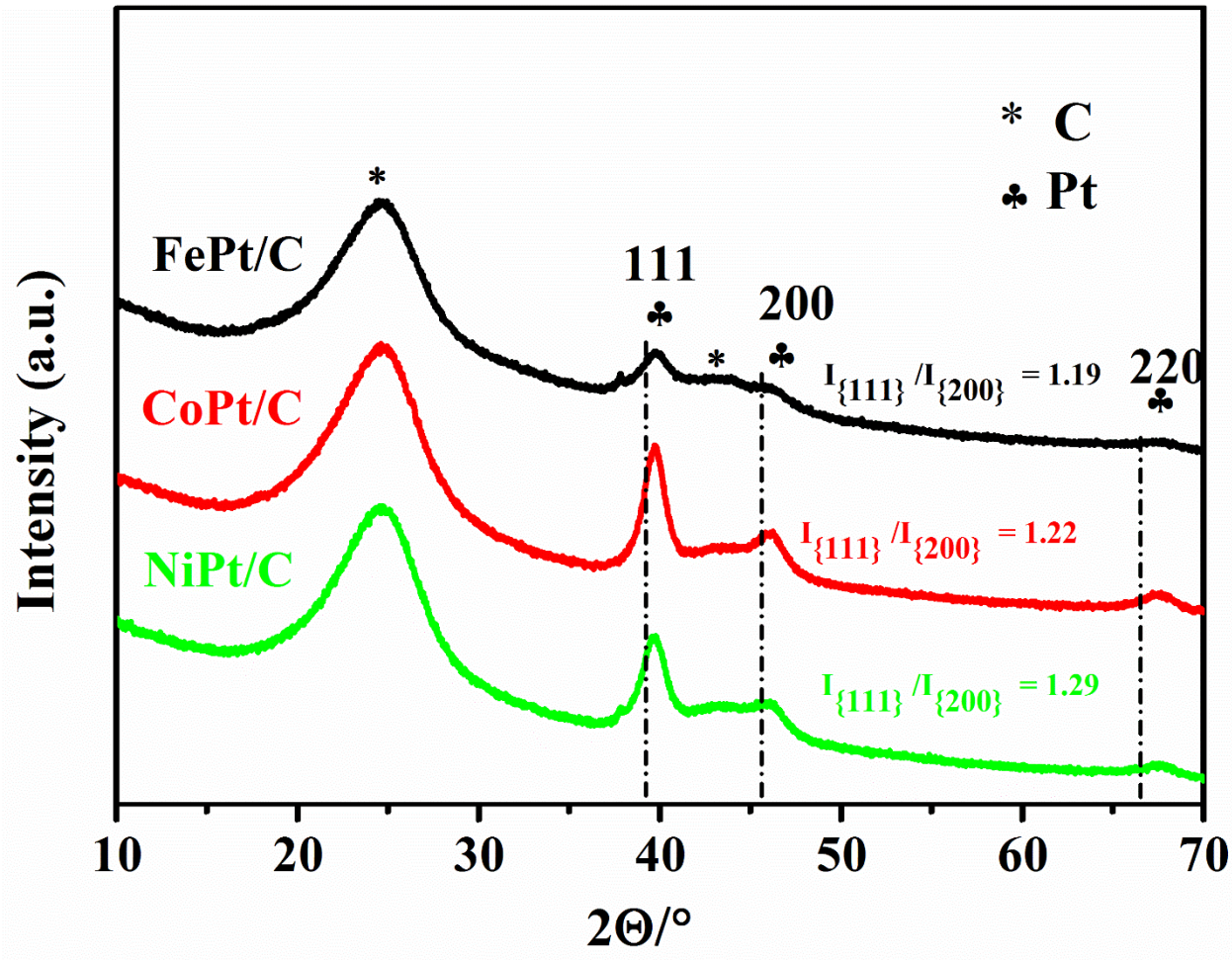

Figure 1. X-ray diffract diagram of the samples: PtFe, PtCo and PtNi alloys. The shown lines, which are parallel to the y-axis, correspond to the pure polycrystalline Pt (dash dot line).

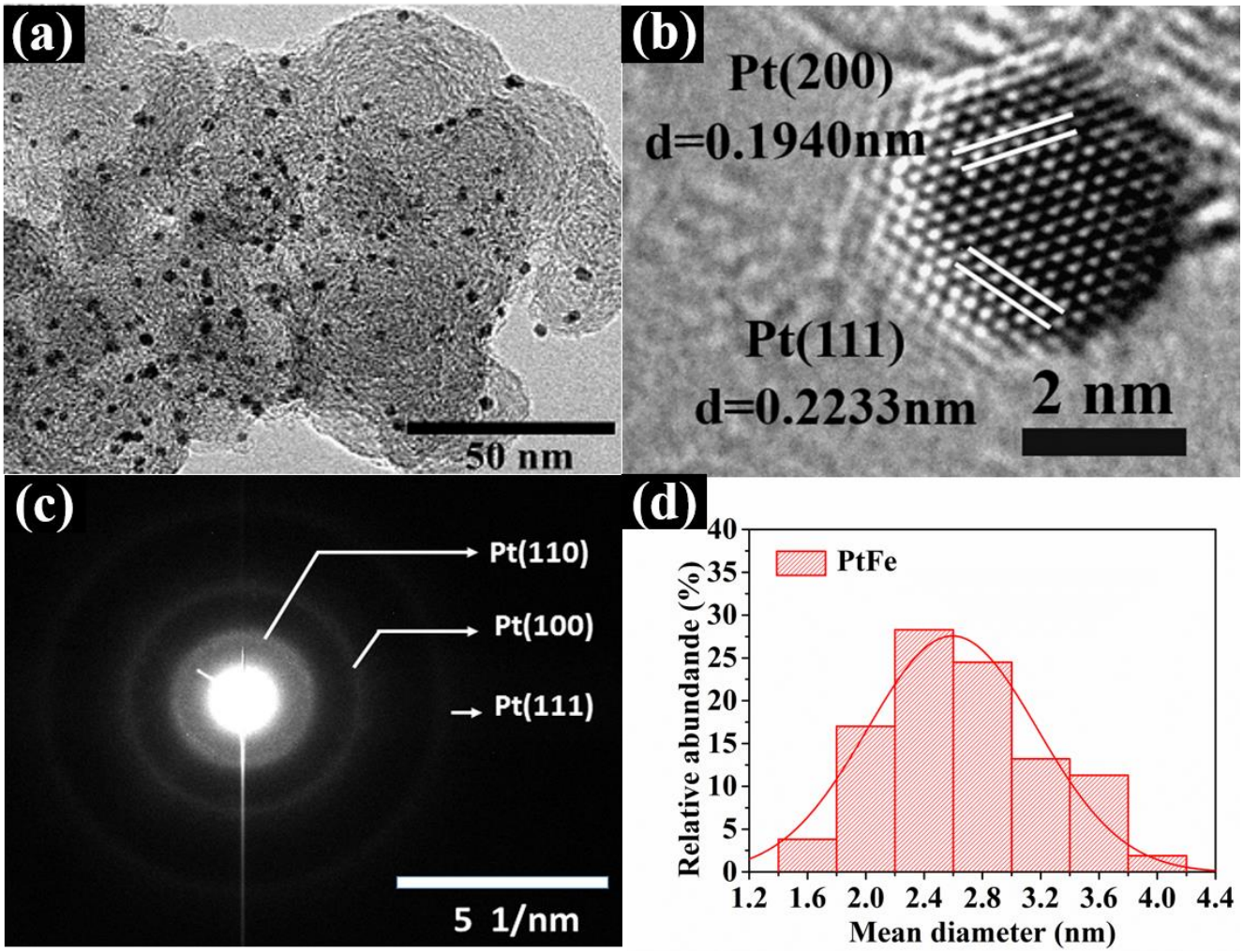

Figure 2. Transmission electron microscopy image (a), micrographs with higher magnification (b) and the corresponding SAED patterns (c) of the PtFe alloy. (d) is the histograms of the average diameter distribution of particle catalysts in 0-5 nm size range.

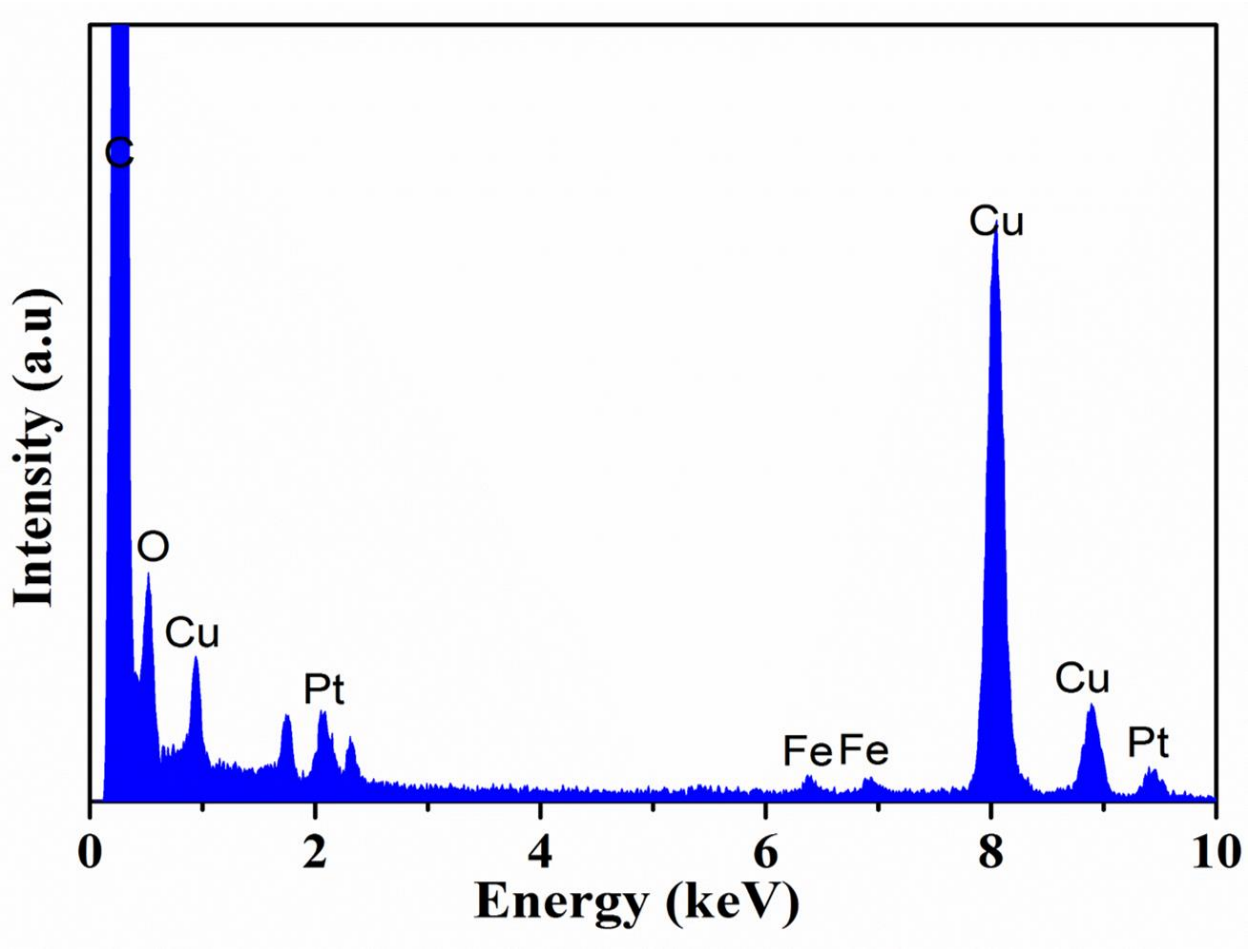

Figure 3. TEM-EDS images of PtFe alloy catalyst prepared by the soft chemistry method.

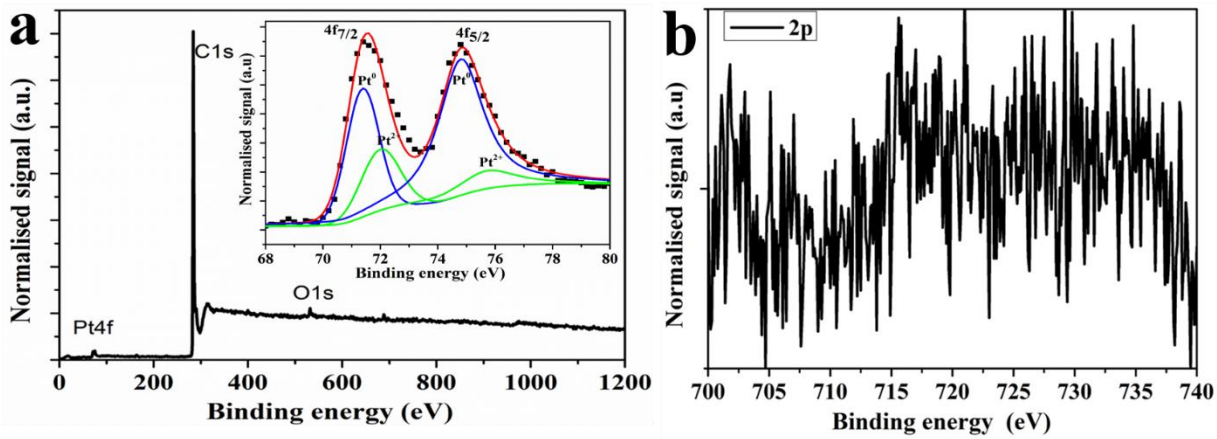

Figure 4. XPS survey for the as-prepared PtFe alloy sample (a), Pt 4f in the inset of (a), and Fe 2p (b).

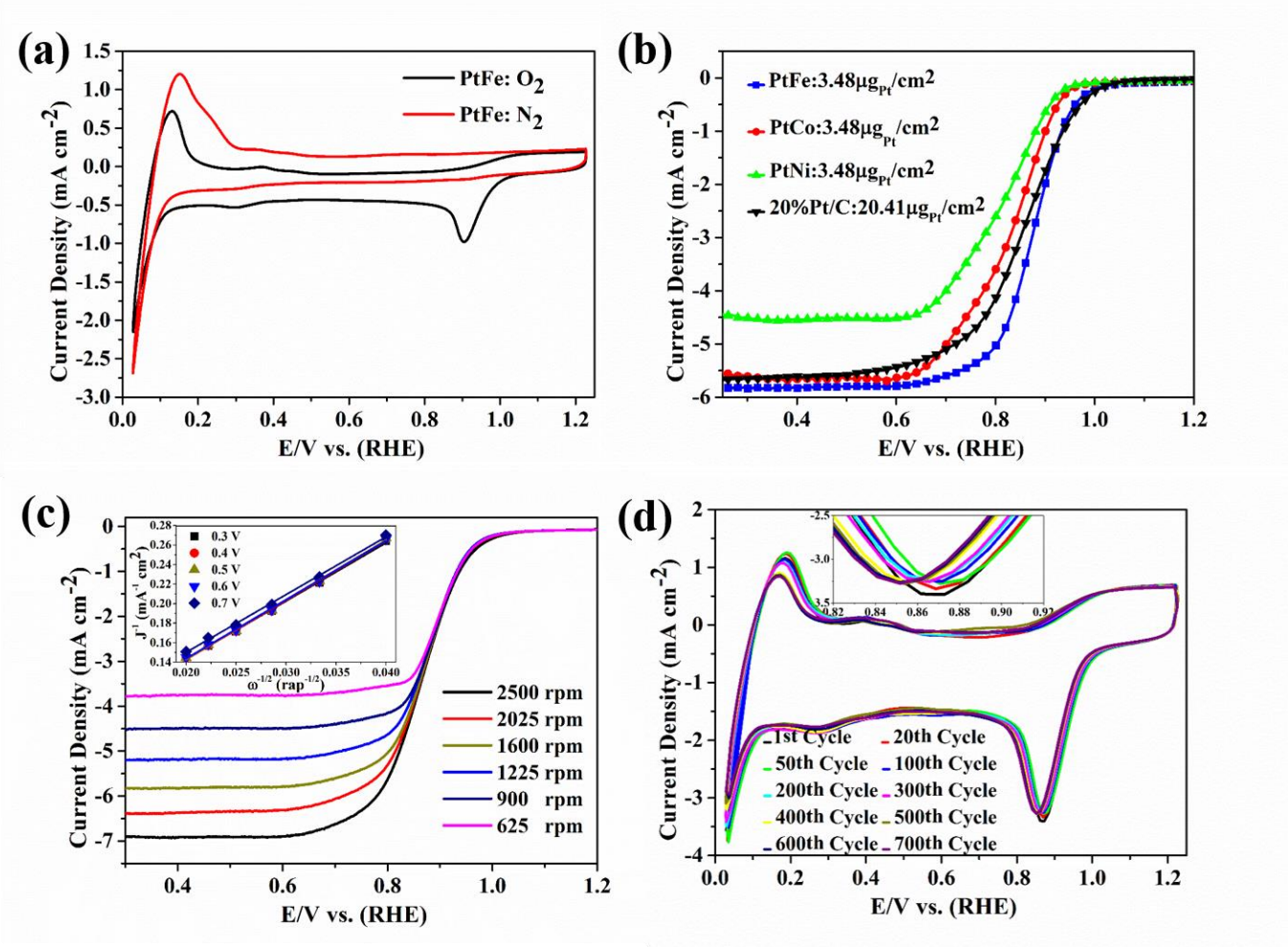

Figure 5. CV curves in nitrogen- and oxygen-saturated solutions without any rotation (a). LSV curves in oxygen–saturated solutions at 1600 rpm for the three samples and the commercial Pt/C (b). LSV curves of the PtFe alloy with the different rotation speeds (c). The K-L plots for the PtFe alloy at the different potentials shown inset of (c). The PtFe alloy sample stability accessed by the CV measurements at a scan rate 50 mV s^{-1} (d). All the test is in the 0.1 M KOH medium.

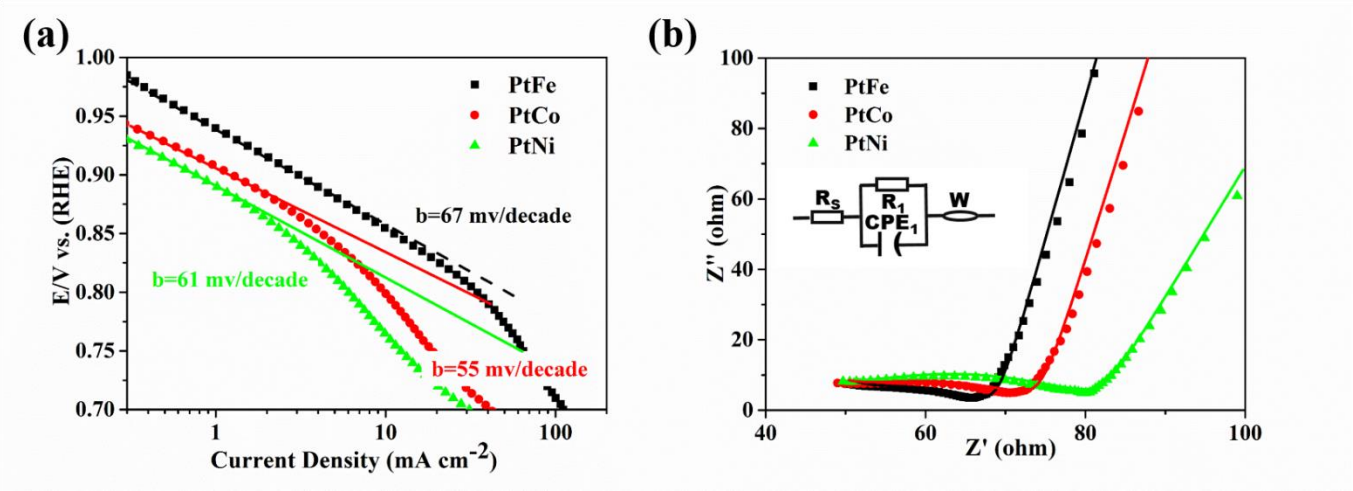

Figure 6. The corresponding Tafel plots from LSV curves at 1600-rpm (a). The impedance spectra of three samples at open circles potential, and the line is the fitting results (b). All the test is in the 0.1 M KOH medium.

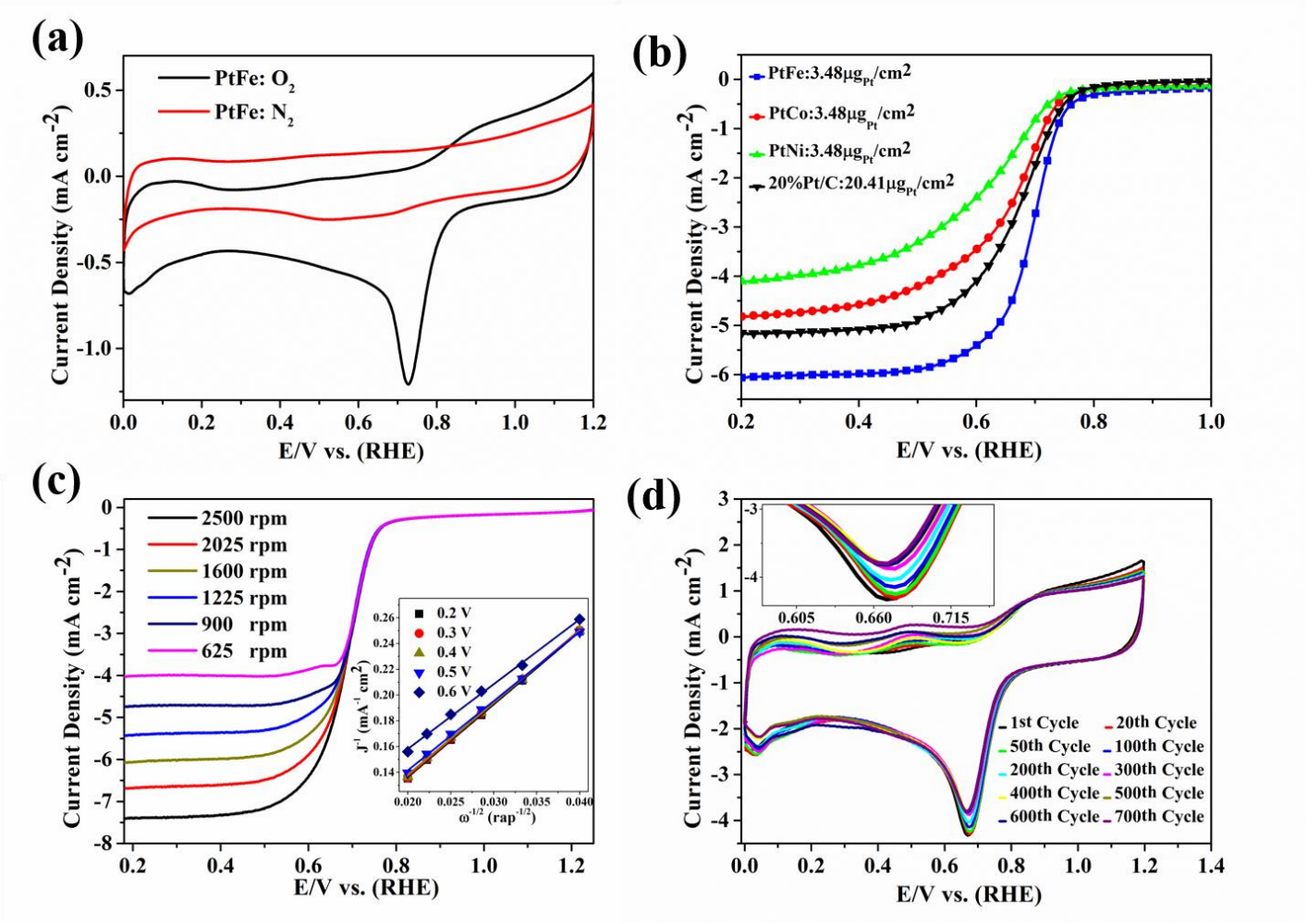

Figure 7. CV curves in nitrogen and oxygen–saturated solutions without any rotation (a). LSV curves in oxygen–saturated solutions at 1600 rpm for the three samples and the commercial Pt/C (b). LSV curves of the PtFe alloy with the different rotation speeds (c). The K-L plots of the PtFe alloy at different potentials shown inset of (c). The PtFe alloy sample stability accessed by the CV measurements at a scan rate 50 mV s^{-1} (d). All the test is in the 0.1 M $HClO_4$ medium.

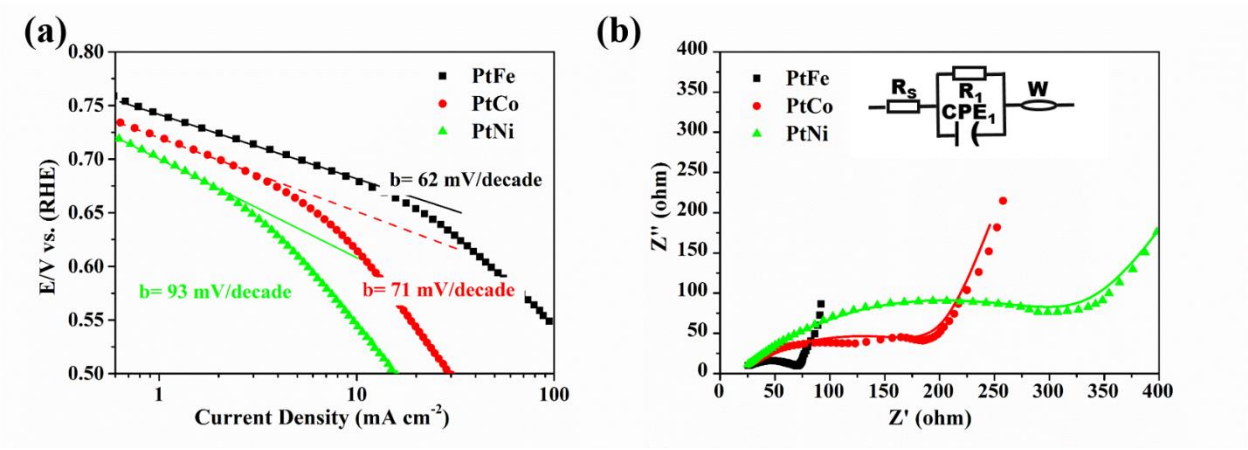

Figure 8. The corresponding Tafel plots from LSV curves at 1600-rpm (a). The impedance spectra of three samples at open circles potential, and the line is the fitting results (b). All the test is in the 0.1 M $HClO_4$ medium.